Biophysical Journal Volume 95 August 2008 1729–1744

Molecular Dynamics Simulation of Kv Channel Voltage Sensor Helix in a Lipid Membrane with Applied Electric Field

Manami Nishizawa and Kazuhisa Nishizawa
Department of Laboratory Medicine, Teikyo University School of Medical Technology, Itabashi, Tokyo, Japan

ABSTRACT In this article, we present the results of the molecular dynamics simulations of amphiphilic helix peptides of 13 amino-acid residues, placed at the lipid-water interface of dipalmitoylphosphatidylcholine bilayers. The peptides are identical with, or are derivatives of, the N-terminal segment of the S4 helix of voltage-dependent K channel KvAP, containing four voltage-sensing arginine residues (R1–R4). Upon changing the direction of the externally applied electric field, the tilt angle of the wild-type peptide changes relative to the lipid-water interface, with the N-terminus heading up with an outward electric field. These movements were not observed using an octane membrane in place of the dipalmitoylphosphatidylcholine membrane, and were markedly suppressed by 1), substituting Phe located one residue before the first arginine (R1) with a hydrophilic residue (Ser, Thr); or 2), changing the periodicity rule of Rs from at-every-third to at-every-fourth position; or 3), replacing R1 with a lysine residue (K). These and other findings suggest that the voltage-dependent movement requires deep positioning of Rs when the resting (inward) electric field is present. Later, we performed simulations of the voltage sensor domain (S1–S4) of Kv1.2 channel. In simulations with a strong electric field (0.1 V/nm or above) and positional restraints on the S1 and S2 helices, S4 movement was observed consisting of displacement along the S4 helix axis and a screwlike axial rotation. Gating-charge-carrying Rs were observed to make serial interactions with E183 in S1 and E226 in S2, in the outer water crevice. A 30-ns-backward simulation started from the open-state model gave rise to a structure similar to the recent resting-state model, with S4 moving vertically ~6.7 Å. The energy landscape around the movement of S4 appears very ragged due to salt bridges formed between gating-charge-carrying residues and negatively charged residues of S1, S2, and S3 helices. Overall, features of S3 and S4 movements are consistent with the recent helical-screw model. Both forward and backward simulations show the presence of at least two stable intermediate structures in which R2 and R3 form salt bridges with E183 or E226, respectively. These structures are the candidates for the states postulated in previous gating kinetic models, such as the Zagotta-Hoshi-Aldrich model, to account for more than one transition step per subunit for activation.

INTRODUCTION

Voltage-gated ion channels open and close in response to changes in transmembrane potential via motion of the voltage sensor domains (1). The voltage-dependent potassium channels, known as Kv channels, are tetramers with each subunit containing six-transmembrane segments, termed S1–S6. Voltage sensor domains consist of four segments—S1, S2, S3, and S4—each containing a transmembrane helix (2–5). A single pore domain is formed by the S5-S6 regions from the four subunits. The movement and conformational change of segments S1–S4 within the voltage sensing domain is somehow coupled to the intracellular gate of the pore domain (S5-S6) to open and close the channel (6). It is now clear that the voltage-sensing S4 segment in voltage-dependent ion channels undergoes movement in response to varying membrane potential (7,8). The S4 helix in each voltage sensor domain has a series of positively charged amino acids at every third position. Four arginine residues (Rs) have been shown to be present on the same side of the S4 helix of the voltage-dependent ion channels, KvAP and Kv1.2 (4,5). Because the recent structure of the mammalian Kv1.2 voltage-gated K^+ channel appears to be activated/open state (5), a number of experimental studies have been carried out and several models for the closed state have been proposed to study the mechanism of voltage-dependent gating that drives resting and activated states. Although it is beyond the scope of this article to review details of experimental and modeling studies, the models include the original paddle model (9), the more recent paddle model (10), the helical screw model (8,11–13), and the transporter model (14).

In these models, it is generally accepted that the S1 and S2 segments do not move extensively upon gating (8,14,15). On the other hand, there is still disagreement concerning how and to what extent the S3 and S4 segments move (7–10,15–20). While many models have been derived taking into account the open state Kv1.2 crystal structure (5), the structural constraints informative for constructing the resting state models remain relatively scarce. (However, see (21).) How a voltage sensor domain interacts with the surrounding lipid bilayer is also a matter of debate and under extensive research (22–25).

Recent advances in force field and computation have allowed increasingly complex systems to be studied, including peptides binding to lipid membranes and, in particular, ion channels within membranes (e.g., 26–29). Atomistic molecular dynamic simulations have been used to explore the

Submitted January 30, 2008, and accepted for publication April 25, 2008.

Address reprint requests to Kazuhisa Nishizawa, Tel.: 81-3-3964-1211; E-mail: kazunet@med.teikyo-u.ac.jp.

Editor: Peter Tieleman.

© 2008 by the Biophysical Society
0006-3495/08/08/1729/16 $2.00

doi: 10.1529/biophysj.108.130658

interactions of a transmembrane S4 helix with a lipid bilayer (30), of a Kv1.2 channel with a lipid bilayer (31,32) and of the KvAP voltage sensor with a detergent micelle (33) and with a lipid bilayer (30).

Before focusing on voltage-sensor dynamics, we were interested in the general physicochemistry of arginine-containing peptides. Several studies have shown differences between arginine (R) and lysine (K) residues in the effect on peptide-lipid membrane interactions. One such area is cell-penetrating peptides, also known as protein transduction domains (34). Cell-penetrating peptides not only can enter cells but also can deliver molecular cargos. Of note, R_9 (a peptide consisting solely of nine Rs), but not K_9, exhibits transduction into cytoplasm (35). Moreover, it has been shown that Tat_{47-57} (YGRKKRRQRRR), a well-known CPP found in Tat protein of HIV virus, and $YG(R)_9$ are transduced to the cytosolic compartment, while $YG(K)_9$ is endocyted and remains in the endosomes (36).

For voltage sensors of voltage-dependent channels, the important gating charges are carried nearly always by R, not K. The delocalization of the positive charges over the side chain of Rs may be important for movement of the voltage sensor (9). Our recent molecular dynamic simulations of positively charged amphipathic peptides HaTx1 and GsMTx4 also showed the smooth movement of R as opposed to K (37).

In our preliminary analyses of the behaviors of R-containing peptides within membrane, we incidentally observed that the N-terminal segment of the S4 helix of KvAP exhibits a tilting movement upon changing the direction of an external electric field. With an interest in general peptide-membrane interactions, we first focus on the dynamics of the N-terminal segments of S4 under varied directions of the electric field. In Results and Discussion, the simulations of S1–S4 within the dipalmitoylphosphatidylcholine (DPPC) lipid bilayer are considered.

SIMULATION DETAILS

The GROMACS 3.3.1 program was used for molecular dynamic simulations. For DPPC, the parameters modified by Tieleman and Berendsen were used (38). For the N-terminal segment of S4, its derivatives, the S4 helix, the voltage sensor (which we refer to as S1–S4), and the GROMOS96 parameter set was used. For water, the simple-point charge (SPC) model was used (39).

The peptide LFR, which is identical to the N-terminal part (115–127) of the S4 helix of KvAP, and its derivatives are listed in Table 1. We chose KvAP because the results of the dynamics simulations of KvAP were available at the time (40,41). The KvAP voltage-sensor crystal structure (PDB ID code 1ORS) (4) was used as the initial coordinates for LFR. The initial coordinates for other peptides were obtained by replacing each residue with the aid of SwissPDBViewer (us.expasy.org/spdbv) and performing energy minimization with harmonically restraining C_α positions. The N- and C-terminus of the peptides were capped with an acetyl group and an NH_2 group, respectively. The initial coordinates of the bilayer membrane consisting of 128 DPPC molecules were taken from the preequilibrated membrane as we described (42). The peptides were placed horizontally at the depth of carbonyl oxygen atoms (with the center of mass of the peptide being 1 nm above that of the lipid membrane). To avoid molecular overlap, the growth method was used; the peptide whose size had been reduced to 1:10 was allowed to grow by energy minimization (43). The peptide/DPPC system was hydrated with 3840 water molecules containing seven sodium and 11 chloride ions. Before the productive runs, a 1-ns equilibration run was carried out with restraints on the peptide atoms. The dihedral angles (ϕ and ψ) were harmonically restrained with the coefficient of 125.6 kJ/mol/(rad)^2 for all production runs of the peptide-membrane system.

TABLE 1 Peptides used for the 13aa peptide/membrane simulations

	τ (°)†		Position from bilayer center (nm)‡	
Peptide (sequence)*	Resting	Activated	Resting	Activated
LFR (Ace-LFRLVRLLRFLRI-NH_2)	106.3 ± 6.8	72.3 ± 7.0	1.10 ± 0.07	1.01 ± 0.11
LF1K (Ace-LF*K*LVRLLRFLRI-NH_2)	88.2 ± 5.2	78.4 ± 6.1	1.08 ± 0.06	1.21 ± 0.03
LFK(Ace-LF*K*LV*K*LL*K*FL*K*I-NH_2)	93.0 ± 4.8	81.8 ± 5.2	1.18 ± 0.07	1.15 ± 0.05
LWR(Ace-L*W*RLVRLLRFLRI-NH_2)	111.4 ± 6.4	77.8 ± 6.0	1.17 ± 0.05	1.26 ± 0.06
LLR(Ace-L*L*RLVRLLRFLRI-NH_2)	100.7 ± 4.4	72.9 ± 7.5	1.01 ± 0.05	1.07 ± 0.05
LVR (Ace-L*V*RLVRLLRFLRI-NH_2)	101.9 ± 5.6	57.0 ± 5.4	1.08 ± 0.06	1.05 ± 0.04
LIR(Ace-L*I*RLVRLLRFLRI-NH_2)	85.5 ± 6.6	77.4 ± 4.4	1.19 ± 0.06	1.23 ± 0.04
LAR (Ace-L*A*RLVRLLRFLRI-NH_2)	89.2 ± 8.6	86.9 ± 6.7	1.13 ± 0.07	1.10 ± 0.09
LSR(Ace-L*S*RLVRLLRFLRI-NH_2)	98.3 ± 5.4	81.8 ± 5.6	1.13 ± 0.07	1.11 ± 0.05
LTR(Ace-L*T*RLVRLLRFLRI-NH_2)	91.4 ± 7.2	83.2 ± 5.1	1.10 ± 0.05	1.12 ± 0.06
LYR(Ace-L*Y*RLVRLLRFLRI-NH_2)	89.9 ± 6.2	86.2 ± 6.8	1.18 ± 0.05	1.16 ± 0.11
LFR4(Ace-*RLF*L*RV*LLRFL*IR*-NH_2)	69.1 ± 6.6	68.4 ± 4.9	1.12 ± 0.04	1.21 ± 0.07

*Residues introduced to modify LFR are underlined.
†Average and SD obtained from the 50 frames covering the final 2-ns period of the 10-ns simulation.
‡Position of the center of mass from the bilayer center.

For the S4/DPPC system, the initial coordinates of S4 were taken from the crystal structure of Kv1.2 (residues 281–316 of chain B, PDB file 2A79). For the S1–S4/DPPC system, the initial coordinates for S1–S4 were taken from those for residues 162–323 of chain B of 2A79. For the atoms whose coordinates have not been determined, the models by the ROSETTA-membrane method and provided by Dr. Yarov-Yarovoy were used (8,44). For the S4 and S1–S4 peptides, both ends were capped and side-chain ionization states were determined based on pK_a calculations performed using the pro-pKa server (http://159.149.163.21:8080/propka_about.htm). For the open model (8), it was predicted that all of the ionizable side chains would be present in their default (at pH 7) ionization states. For the closed model, although only E236 exhibited an unusually high pK_a (~9.2) for Glu, coordinates sampled from our equilibrium simulation all exhibited a value of ~3–5, and therefore we chose the default ionization pattern for all residues. All histidine residues were set at neutral.

To embed the S4 segment in the DPPC membrane, we used our own program to remove the DPPC molecules that overlapped the protein. For the S4/DPPC system, four DPPC molecules were thus removed and, for the S1–S4/DPPC system, 25 DPPC molecules were removed. The vertical position of S1–S4 was set considering the previous simulation (31), but in our condition the choice of the initial depth of S1–S4 in the membrane was not critical. Our final system for the S4/DPPC simulation was composed of the S4 peptide, 124 DPPC, 4 sodium ions, 11 chloride ions, and 3840 SPC water molecules and for the S1–S4/DPPC simulation the system consisted of the S1–S4 peptide, 104 DPPC, 10 sodium ions, 10 chloride ions, and 5430 SPC water molecules. The typical size of the simulation box for the S1–S4/DPPC system was $64 \times 64 \times 80$ (Å^3).

For all the simulations in this study, the bond lengths were constrained using the LINCS (45). The cutoff for the Lennard-Jones interactions was set at 9 Å. To account for the long-range electrostatic interactions under the periodic boundary condition, the particle-mesh Ewald (PME) algorithm (46) was used with the real-space cutoff at 9 Å and the maximal grid size of 0.12 Å. The integration time-step was set at 2 fs. For peptide/DPPC and S4/DPPC systems, the temperature was set at 323 K, whereas for the S1–S4/DPPC simulations, the temperature was set at 350 K (with the exception of sim-1 for which 323 K was used) with Berendsen coupling (47). The pressure was controlled by the Berendsen barostat at 1 atm with the independent (semiisotropic) coupling in the *xy* and *z* directions. Typically, the first 10 nanoseconds of a simulation was carried out without an external electric field at which point the simulation was continued in the presence of an electric field. Unless otherwise noted, after the energy-minimization without restraints, an equilibration run was carried out for 1 ns constraining the peptide C_α, followed by a free productive run. Analysis of the properties of the system and movement of the peptide was done using a combination of GROMACS utilities and our own analysis programs. We define the τ-angle as the angle between the helix long axis and the *z* axis, which is set to be the membrane normal. Here, the long axis of a helix consisting of *N* residues was defined based on the mean position of the C_α of the i^{th} residue relative to that of the $(i + 7)^{th}$ residue, for which *i* was varied from 1 to $N-7$.

To find a clear trend in a short computation time, we initially applied an electric field of 0.2 V/nm for the peptide/DPPC simulation. For the S4/DPPC and S1–S4/DPPC simulations, we applied external electric fields of 0.2, 0.1, and 0.05 V/nm. We refer to the external electric field in the direction of the *z* axis (mimicking membrane depolarization) as the outward electric field and the direction opposite to the *z* axis as the inward electric field. For S1–S4/DPPC simulations, we also use the terms forward and backward. Forward means that the simulation is started from the resting state model (8) in the presence of the outward electric field so that S4 moves outward, undergoing a transition to the open state. Backward means that the simulation is started from the open state model in the presence of the inward electric field.

Each charged atom feels a local field that is the sum of the applied external field and the field due to the charges of neighboring atoms (48,49). Computation of the electrostatic potential $\phi(\mathbf{r})$ was carried out using the PME method through a modified version of the VMD plug-in *PMEPot* (50,51). The atomic (partial) charges were summed using the Poisson equation

$$\nabla^2\phi(\mathbf{r}) = -4\pi\sum_i \rho_i(\mathbf{r}),$$

where $\rho_i(\mathbf{r})$ is the point charge of atom *i* at position $\mathbf{r}$ being approximated by a spherical Gaussian of inverse width β. The sum was taken over all atoms in the system. The value β was set at 0.25 Å and a density of grid points of $1/(0.8 \times 0.8 \times 0.8$ Å$^3)$ was used. The linear external electric field was added to potential maps as described (49). The term gating-current denotes the movement of charged particles driven by the electric field and necessary for voltage-dependent gating of voltage-dependent channels (1). For Kv channels, the S4 helix carries many of the charged particles, or gating charges. While each of the R and K residues (of S4) carrying gating charges is likely to be ionized $+1e$, these residues move through just a fraction of the total electric field in the membrane. Therefore, as in the literature (e.g., (1,32)), we use the term gating charge to denote the fraction of the total electric field through which each charged residue moves. For example, if a particle with $+1e$ moves down through a half of the total transmembrane electric field, we state that the particle carries the gating charge of $0.5e$. To infer the gating charge carried by each charged residue, R1 for example, we need to know the potential drop that R1 undergoes during voltage-sensing. To this end, we calculated the potential $\phi(\mathbf{r})_{R1}$, which is the potential map calculated and averaged over 100 frames covering an additional 5-ns simulation in which the charges belonging to the R1 residue are turned off.

For example, we calculated the gating charge (i.e., the fraction of the total electric field in the membrane) carried by R1 based on

$$\left\{ \sum_{i} z_i * (\phi(\mathbf{r}_i)_{R1,open} - \phi(\mathbf{r}_i)_{R1,semiclosed}) \right\} \Big/ \left\{ \sum_{i} z_i * E \right\},$$

where the summation was taken for all the atoms belonging to the residue R1, z_i is the charge z of atom i belonging to R1, $\phi(\mathbf{r}_i)_{R1,open}$ denotes the electric potential (at the position of i) created by all the atoms not belonging to R1, and E is the full membrane potential, for which we simply used the product of the height of the simulation box and the strength of the applied electric field. To turn off the R1 charges, a deprotonated arginine residue was used. (Although our experience is currently limited to deprotonation, turning off all the partial charges of the arginine residue may also be considered in the future.) Note that, in addition to C_α movements, side-chain movements of charged residues can contribute to the gating current. Therefore, the potential map $\phi(\mathbf{r}_i)_{R1,open}$ was calculated from a 5-ns simulation, in which 1), all atoms of S4 and charged atoms of DPPC molecules were restrained at the open configuration (the conformation obtained under a depolarizing electric field); and 2), an inward electric field was applied. Namely, an open state/inward voltage simulation. Finally the applied electric field was added to the potential map as described in Sotomayor et al. (49). Similarly, we calculated $\phi(\mathbf{r}_i)_{R1,semiclosed}$ from a 5-ns simulation starting with a semiclosed structure (described below) and an inward electric field, and continued with the restraints on C_α-values of S4 and the inwardly applied electric field: namely, a semiclosed state/inward voltage simulation. While we used explicit treatment of atoms, our approach is similar to the literature (8,32) in which the continuum electrostatic approximation was used for the $\phi(\mathbf{r}_i)$. In our case, the effect of side-chain movements due to an applied electric field can be taken into account to some extent.

Before beginning this study, we carried out several simulations of a dual-bilayer system containing different numbers of ions producing a physiological transmembrane potential (52). We found that the potential map became stable at ~5 ns of equilibrium simulations (M. Nishizawa and K. Nishizawa, unpublished result). Because of the high dielectric coefficient of the water layer, the voltage drop was found to occur only in the hydrophobic interior of the membrane (51,52). The convergence and reproducibility of the transmembrane potential map was not appreciably affected by changing the number of sodium and chloride ions within the range of 10–20 per simulation box. We also performed a simulation of a single bilayer system similar to that of Sotomayor (49) and the *PMEpot* calculation on a 2-ns trajectory showed good convergence after the initial ~5 ns.

Calculations were carried out on 15 desktop PCs with AMD 2.2-GHz processors with or without parallelization. All molecular images were made with VMD (50).

RESULTS AND DISCUSSION

First, we analyzed the effect of an applied electrical field on the behavior of the arginine-containing peptides at the membrane-water interface. Table 1 shows the list of peptides analyzed. LFR is the N-terminus segment of the voltage sensor S4 of KvAP (residues 115–127) forming a helix (4). Our previous simulations starting from different LFR orientations (both in τ and the rotational angle around the helix axis) and positions (depth) exhibited immediate, robust transformation reaching the equilibrium position/orientation within ~1 ns. As was anticipated from its amphiphilicity, LFR moved to a relatively deep part of the lipid headgroup (carbonyl oxygen layer), with the center of mass approaching ~1 nm above the bilayer center.

Fig. 1 shows the average z position of the C_α-values of the peptides over the final 2-ns period of the representative 10-ns simulation. Error bars representing the SD for the 20 frames from the 2-ns period are small. By repeating the 10-ns simulation at least three times, we found that the results were reproducible. LFR exhibited a change in orientation in response to the change in the electric field direction. With the inward electric field (mimicking the resting potential), LFR headed down, with its N-terminus located close to the bilayer center and the C-terminus 1.5 nm above the bilayer center. (Table 1 summarizes the τ-angle.) In contrast, with the outward electric field, LFR headed up, with its N-terminus located >1 nm above the bilayer center and the C-terminus located at a deep position in the membrane. Qualitatively, such voltage-dependent motions can be considered to be caused by interactions between the electric field and the dipole moment of the α-helix; due to the hydrogen bonds formed along the helix axis, the N-terminus has a net positive charge and C-terminus has a net positive charge.

Intriguingly, the magnitude of the motion caused by the electric field change was partly lost when R1 (R117 of KvAP, the first gating-charge-carrying arginine corresponding to R294 of Kv1.2) was replaced with K (LF1K, shown on the *third line* of Fig. 1). Note that R1 is the third residue of the LFR. For LF1K, the N-terminus was located >1 nm above the bilayer center even with the inward electric field and the magnitude of reorientation caused by the electric field change was small. When all four Rs were substituted with Ks, the reorientation due to the electric field change was largely lost (LFK of Fig. 1).

An octane slab/water system has been used in several simulation studies of lipid/peptide interactions (e.g., (26,40)). We examined the LFR and LFK in a box containing 301 octane molecules, 2460 water molecules, and three sodium and seven chloride ions. Neither LFR nor LFK exhibited an appreciable level of voltage-dependent movement (Fig. 1, *bottom*). In both cases, the four positively charged residues extended their side chain into the water layer. Because the electric field is small, we reason that, once the charged residues are trapped in the water, the electric field at the side

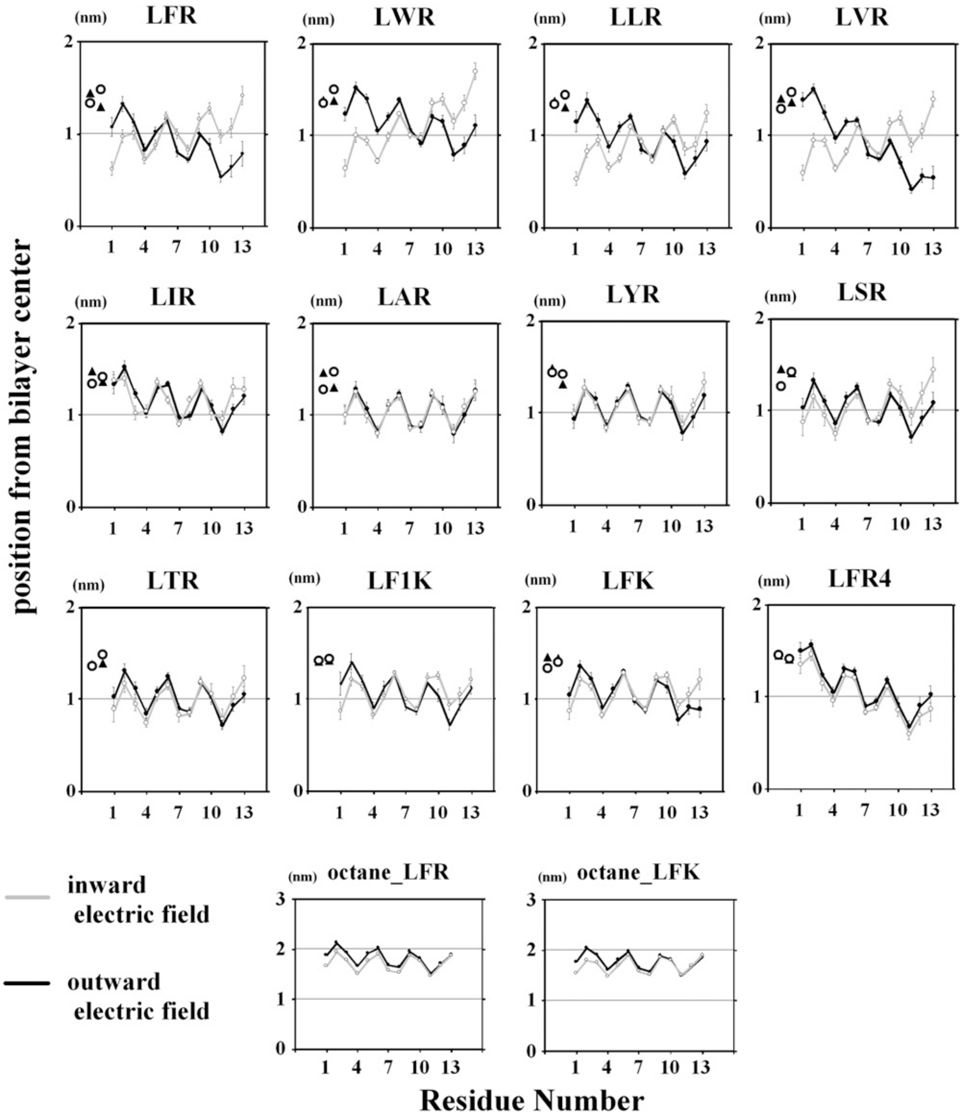

FIGURE 1 The z distance of each C_α in the 13aa α-helix peptides from the DPPC bilayer (*top three lines*) and octane (*bottom*) midplane. For LFR (*top, left*) and LFK (*third line*), one representative trajectory out of five 10-ns simulations was analyzed. For the other peptides, one out of three runs was analyzed. Shown is the position averaged from 20 frames covering the final 2-ns period of the simulation. Error bars show the mean $\pm$ SD for the 20 frames. Shaded lines show the results with the inward (resting) electric field. Dark lines show the results with the outward (depolarizing) electric field. Symbols shown in the left part of each graph show the mean z position of the center of mass of the carbonyl oxygen atoms (COs) in the outer membrane leaflet in simulations performed with an inward electric field (*circle*) and an outward electric field (*solid triangle*). The left-most symbols indicate the center of mass of the COs at least 0.7 nm away from any atoms in the peptide, whereas the symbols just to the right of them indicate the com of COs located within 0.7 nm of any atoms in the peptide. For the peptide/octane system (*bottom*), the mean $\pm$ SD was negligibly small ($<\sim$0.1 nm), and so omitted.

chains becomes so weak in the high dielectric coefficient of water that the movements are lost.

Why does R, but not K, enable the peptide to respond to the electric field change? Visual inspection indicates that, in the absence of the external electric field, R1 (R117 in KvAP, corresponding to R294 in Kv1.2) and R4 (R126 in KvAP and R303 in Kv1.2) of LFR were located at approximately the depth of OSs, which is relatively deep among the lipid headgroup atoms. (Note that oxygen atoms in the carboxyl ester of DPPC can be classified into two groups: 1), the carbonyl oxygen atoms—O_{16} and O_{35} or OC—that are linked solely to the carbon atom of carboxyl groups; and 2), the ester oxygen atoms—O_{14} and O_{33} or OS—that are linked directly to glycerol backbone of the phosphatidyl group.) On the other hand, as exemplified by LF1K, K tends to form hydrogen bonds with phosphate and water oxygen atoms. It was also shown that LFK is located at a more outward (shallow) position than LFR (Table 1). Thus, R and K behave differently in the hydrogen-bond formation with the lipid headgroup. We will focus on the hydrogen-bond partners of R1 in the next subsection.

We also noticed that Phe^2, which is located just before R1, behaved unusually; despite its hydrophobicity, Phe^2 protruded into the water layer. For most of the simulation time, we did not observe interactions typical of the cation-π effect between Phe^2 and R1, but the side chain of Phe^2 was usually located close to that of R1. Fig. 2 shows a typical snapshot at the inward and outward electric field. To gain more insight, we replaced Phe^2 with other types of amino acids (Fig. 1). LSR and LTR did not show the electric field-dependent movement. In contrast, LWR, LLR, and LVR exhibited reorientation similar to LFR. These results suggest the hydrophobicity of the second residue and perhaps the depth of the N-terminus at the resting potential is crucial for the large magnitude movement associated with the electric field change. It seems possible that the second (hydrophobic)

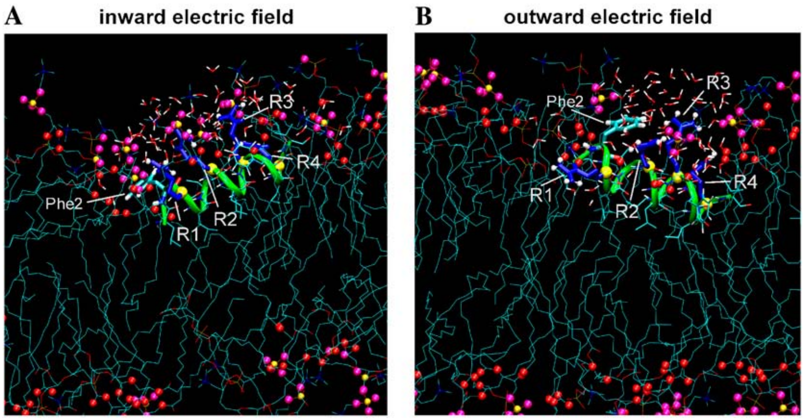

FIGURE 2 Snapshot of LFR/DPPC. Shown are frames at 10 ns of the simulation with the inward (*A*) and the outward (*B*) electric field. For clarity, Phe^2 and four Rs are shown in licorice representation. Green ribbon shows the backbone of the LFR peptide, whereas yellow spheres show the C_α-values of R1–R4.

residue may limit hydration of R1, mitigating the charge-masking effect of water.

It is interesting that hydrophilic residues (S and T) do not bring the N-terminus to a position as high as in LFR (and LWR, LLR and LVR) with the outward (activated) electric field. It could be that S or T and water molecules hydrating S and T reduce the effective charge of R1. Because the magnitude of movement of LAR was small, the bulkiness of the second residue could also be an important factor for the wide range of movement at the activated potential.

For LFR4, four residues were replaced with R, not at every third, but at every fourth residue. With this interval, the four Rs lie on the same side of the helix, aligned along the long axis of the helix. Despite that the amino-acid composition of LFR4 is the same as LFR, LFR4 did not exhibit an appreciable degree of voltage dependent movement (Fig. 1, *third line*). It is most likely that, because the four Rs are aligned on one side of the helix, R1 of LFR4 may be located at a high position and therefore, lose access to the deep oxygen atoms, which would otherwise act as scaffolding for these movements.

Carbonyl and ester oxygen atoms of DPPC

Intriguingly, when R1 is located deeper in the lipid headgroups, it forms hydrogen bonds with OSs as well as with OCs. By contrast, when R1 is located in a shallower position (as in the case with an outward electric field), R1 forms more hydrogen bonds with water and phosphate oxygen atoms (Fig. S1 in Supplementary Material). The situation was different in the case of K. K in place of R1 forms hydrogen bonds mainly with OCs both at the resting and activated potentials and there was a relatively small change in hydrogen bond partners upon the electric field change (LF1K, LFK, and Fig. S1, *third line*). Given that R-to-K substitution leads to shallow positioning of the peptide (e.g., *LFK* of Fig. 1 and Table 1), it is possible that the restrictive nature of K may be caused by its preferred hydrogen-bond formation with OCs and water molecules, disfavoring interactions with phosphate group. By contrast, R appears to interact with various oxygen atoms with fairly similar frequency, and this may partly facilitate the large magnitude of motion of R-containing peptides upon the change in the electric field. However, it should be noted that the force field used in this study assigns relatively large negative atomic charges to OS and OC atoms. More analyses are necessary to examine the robustness of these results (i.e., the prevalent involvement of OCs in hydrogen-bond formation and the difference between R and K) with respect to the choice of force fields. Although we used DPPC only, it may also be important to examine different compositions of lipid.

For the group of peptides exhibiting a marked reorientation (LFR, LLR, LWR, and LVR), the number of phosphate oxygen atoms forming hydrogen bonds with R1 increased with the outward electric field (Fig. S1). For those peptides exhibiting an insignificant level of reorientation (LAR, LYR, LSR, and LTR), no substantial increase in hydrogen bonds between R1 and phosphate oxygen atoms was observed upon applying the outward electric field. Of note, LSR and LTR, even with an inward electric field, form hydrogen bonds with phosphate oxygen atoms. LFR4 hydrogen-bonds to phosphate oxygen atoms but hydrogen-bond partners were not affected by the change in electric field. These results suggest that phosphate oxygen atoms play a role as the outermost scaffolding for the peptide motion; phosphate oxygen atoms may be reserved for the depolarized membrane potential if large movements like the ones seen with LFR, LLR, LWR, and LVR are to be enabled.

S4 helix simulation

Based on the apparent free energy of translocon-mediated integration of transmembrane helices into the endoplasmic reticulum membrane (53), it has been argued that the S4 helix can be inserted into a membrane without other peptides or peptide segments (54). Although S4 helix is likely to be accompanied by other helices in physiologically relevant situations, it is of physicochemical interest to interpret the results of the S4 helix that have been reported in Hessa et al. (54). The S4 helix of KvAP in the transmembrane configuration has also been analyzed by molecular dynamic simulations

(41). While the vertical orientation of S4 with respect to the membrane persisted through the simulation (41), the total simulation time was considerably short (∼10 ns). We carried out several 10-ns simulations using S4 of Kv1.2. S4 movement appeared to depend on the initial position. When we placed S4 at the height of the bilayer center, S4 exhibited a 4.3 Å inward movement (Fig. 3 *A*). When S4 was placed at 4.5 Å above the bilayer center, a ∼2 Å inward movement was observed (Fig. 3 *B*). The charged residues interact strongly with either the outer or the inner lipid headgroups, and it seems that S4 cannot search the equilibrium position quickly. Intriguingly, unlike the previous result (41), the S4 helix, which was placed in the nearly vertical orientation, began tilting and the τ-angle increased for the initial 3 ns, and finally reached ∼50° (Fig. 3, *A* and *B*). The resultant S4 orientation was somewhat similar to that observed in the S1–S4 simulations described below, but the side chains of Rs interact with the lipid headgroups, causing membrane thinning. For Fig. 3, simulations were performed with a 0.05 V/nm inward electric field, but the tilting was reproduced without the external electric field (data not shown). Note that all atoms of S4 were initially position-restrained, allowing us to evaluate flexibility of the membrane (*left panels* of Fig. 3). After the restraints were turned off, the tilting began but the membrane deformation largely remained (*right panels* of Fig. 3, *A* and *B*). When we placed S4 in a manner mimicking the x-ray structure by Long et al. (5), the S4 helix started to bend at ∼1 ns and was disrupted (Fig. 3 *C*). (For the simulations shown in Fig. 3, we did not introduce restraints on the dihedral angles of peptide backbone.)

The measurement by Dorairaj and Allen (55) has shown that the free energy of polyleucine α-helix with an arginine residue near the center of the membrane is high (∼70 kJ/mol). Therefore, the oblique orientation of the S4 helix, which appears to facilitate the interactions between Rs and the lipid headgroups, may represent a more stable orientation than the vertical orientation that was reported in Freites et al. (41). Previous attenuated total reflection-Fourier transform infrared spectroscopy studies have shown that the S4 segment of *Shaker* (with the sequence LAILRVIRLVRVFRIFKLSRHSKGLQ, 26 residues) is oriented parallel to the membrane surface, with τ being 70–72° (56). Solution and solid-state NMR spectroscopy analyses have also shown that the S4 segment of the rat brain sodium channel (with the sequence ALRTFRVLRALKTISVIPGLK, 21 residues) is oriented approximately parallel to the membrane surfaces of

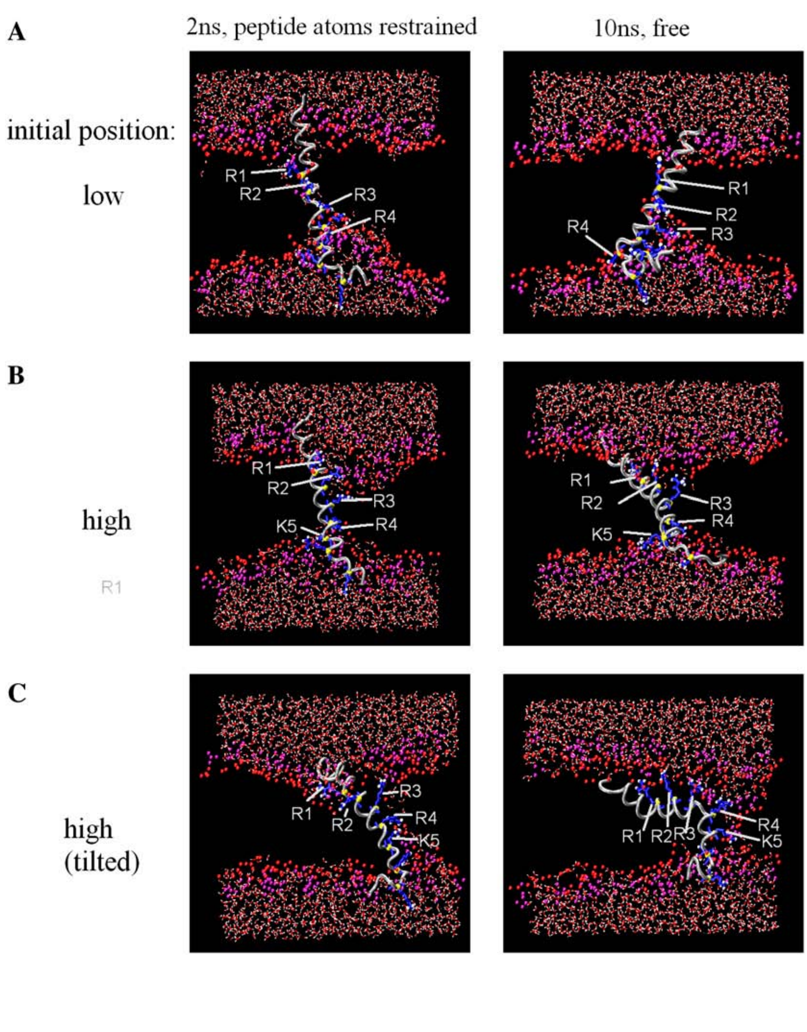

FIGURE 3 Snapshots of S4 simulations. (*A*) Simulation with S4 initially placed at a low position. The center of mass (or com) of R1–R4 C_α-values was placed −0.029 A above the bilayer center. (*B*) Simulation with S4 initially placed at a high position. The com was placed 4.5 Å above the bilayer center. (*C*) Simulation with S4 initially placed at a high position and tilted. The com was placed 4.2 Å above the bilayer center and the τ-angle was set at 43° to mimic the x-ray structure reported by Long et al. (5). For each of panels *A–C*, left snapshot is the frame at 2 ns of simulation with the positional restraints on all atoms of S4 helix. Right snapshot is the frame obtained 10 ns after the restraints were removed. The peptide backbone is shown with a silver tube. Red spheres, ester oxygen atoms; purple spheres, phosphate oxygen atoms.

dodecylphosphocholine micelles and a planar palmitoyl phosphatidylcholine bilayer (57). It thus seems quite possible that the isolated S4 helix favors interfacial position, assuming an orientation parallel to the membrane surface. Our data favor the view that, for an isolated S4 helix, the true minimum in the free energy surface is likely to involve an interfacial configuration (58,59), although computational analyses of an isolated S4 are difficult at present because of the long simulation time necessary for equilibration.

The argument of the S4 helix insertion into the membrane (54) was based on the number of glycosylation events on the nascent S4 peptide; glycosylated only once is interpreted to mean that the helix was membrane-inserted, whereas glycosylated twice is interpreted to mean that the helix was not (60). However, oligosaccharyl transferase (OT) complex, which is responsible to the glycosylation, directly interacts with the translocon protein complex (e.g., 61) and therefore, position of the peptide relative to the translocon complex should affect glycosylation rates and efficacy (60). OT complex has been estimated to be 120 Å in heights, and, assuming the 40 Å embedded on the lipid bilayer, the height of the part protruding into the endoplasmic reticulum (ER) lumen is estimated to be ~40 Å (62). It has also been shown that the active site of OT complex is located ~30–40 Å away from the membrane in the ER lumen (63). One of the glycosylation sites introduced into the plasmid system of Hessa et al. (54) is close to the C-terminus end of the tested peptide (with their interval being only five residues according to (53)). Considering this, the S4 helix could temporarily settle into a position within the translocon that permits only a single glycosylation event, and end up adopting a helical configuration parallel to the membrane surface (60).

S1–S4 simulations

Voltage-sensing domains have recently been described in voltage-sensing proteins that lack associated pore domains (64–66). In the voltage-activated proton channel (mVSOP or alternatively called Hv1), the voltage-sensing domain itself is thought to function as a proton channel (65,66). It is reasonable to assume that the voltage-sensing domains are modular and they can function as a unit independent from the pore-forming domains (S5-S6). We performed simulations of the voltage sensor domain (S1–S4) of Kv1.2. When we performed a simulation without restraints on helices, the whole structure of S1–S4 underwent a conformational drift, which was associated with concerted movements of membrane lipid. Although the drift could be informative, we chose to restrain S1 and S2 by positional harmonic restraints on C_α-values so that we could easily evaluate the S3 and S4 movements. The restraints could also be beneficial in preserving the overall conformation, given the harsh conditions adopted in the following simulations (see below). Note that it is well established that the movement of S1 and S2, relative to the whole S1–S4 structure, upon gating is negligible (e.g., (8,14)).

We first performed several simulations starting from the open state model (8) without applying the electric field. Water molecules filled the small crevices above and below R4 (R303), forming an hourglass-shaped aqueous region (the initial frame of Movie 1 of our site at http://homepage3.nifty.com/~gene). Similar structures have been reported in the simulations of Kv1.2 (31,32) and of the isolated voltage sensor of the KvAP channel (30,33). As typical snapshots show, R1 and R2 are positioned to interact with a mixed lipid-water environment and the water environment of the external aqueous cleft, respectively (Movie 1 of our site). That R1 and R2, in the open state, interact with water molecules as well as lipid headgroups is also shown by the hydrogen-bond partner analysis and cumulative radial distribution function analysis (data not shown). For most of the simulation time, R3 and R4 formed salt bridges with E183 (of S1) and E226 (of S2), respectively (Fig. 4 *A*). R3 was also competing with R4 for E226. These interactions have been pointed out in the x-ray structure study (10).

Even without restraints on S3, S3 remained close to S2 near the intracellular side. K5 (K306 of S4) maintained in-

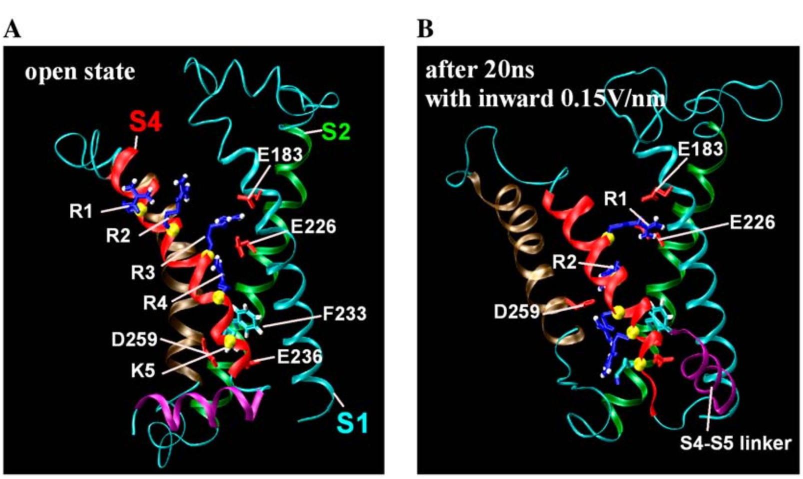

FIGURE 4 Conformation changes observed in simulation-5 (sim-5). (*A*) Snapshot after 1 ns of the simulation without the electric field. (*B*) Snapshot after 20 ns of the simulation in the presence of the inward electric field at 0.15 V/nm (see Table 2).

teraction with both D259 (of S3) and E236 (of S2), acting as glue keeping the helices close together. This is consistent with the experimental findings in the second-site suppressor analysis of the *Shaker* B channel (67), which shows that D259 and E236 are electrostatically interacting with K5.

Based on methanethiosulfonate reactivity of site-directed cysteines in the *Shaker* K^+ channel, it has been shown that R3, R4, and K5 are inaccessible in the open state and become accessible from the inside in the resting state (68). The latter finding led the authors to suggest a large inward translocation of S4 and/or a wide opening of the voltage sensor to the inside (widening the intracellular vestibule). Our open-state simulation showed a somewhat wider opening of the intracellular vestibule than the open state model by Pathak et al. (8), but Phe^{233} acted as a barrier that prevents water penetration from the intracellular side. The opening was even wider when the inward electric field was applied as shown below. Although this is consistent with the methanethiosulfonate-accessibility data, it is not clear whether or not our simulation is reliable in evaluating the width of the opening to the intracellular side, given the strong electric field and the truncation on the S5-S6.

S4 movement with inward electric field

We continued the simulation, applying the different strengths of electric field (Table 2). For sim-1 and -2, an inward electric field of 0.05 V/nm was applied. Despite the high temperature (323 K for sim-1 and 350 K for sim-2), the displacement of S4 helix was insignificant even at 30 ns (see also Fig. 6). Table 2 shows the magnitude of vertical translocation of C_α and the side-chain carbon-atom (CZ, the closest carbon atom to the charged nitrogen atoms) of the gating-charge-carrying residues of S4. When we applied a strong inward electric field (0.2 V/nm), the membrane broke apart and a water pore occurred (sim-7 and -8).

Strikingly, for sim-5, in which an inward 0.15 V/nm electric field was applied, S4 moved ~6.7 Å inward and R1 formed salt bridges with E183 and E226 at 12 ns (Figs. 5 and 6 and Table 2). We tentatively call the structure at 30 ns of sim-5 the semiclosed structure. As Movie 1 (of our site) shows, S4 exhibited a screwlike (i.e., axial) rotation of ~90°, which was counterclockwise when viewed from the extracellular side.

In general, when the applied electric field was weak (0.1 V/nm or 0.05 V/nm), the S4 translocation was small (e.g., sim-1 to sim-4 of Table 2, Fig. 6). It is also noted that the side chain of the gating-charge-carrying Rs exhibited larger movements than the C_α-values.

Salt bridge formation appeared to be the major factor slowing the S4 movement. The initial (open-state) conformation places R4 in the vicinity of the E226 of S2 (Fig. 4 *A*). Typically, during the initial ~1 ns, R3 replaced R4 to form a salt bridge with E226, although for sim-1, R3 was interacting with E183 at the end of the simulation (30 ns). For many simulations, even after a slight inward movement of S4 (over 2 Å), the R3-E226 salt bridge remained stable (Fig. 5, *A* and *B*; Fig. 6; and Movie 1). For sim-2 and sim-6, the R3-E226 remained until the end of the simulation. Although the time point was different among the simulations, the R3-E226 salt bridge finally broke apart and, in turn, R2 formed a salt bridge with E226. Such transitions occurred abruptly. Close to the same time, R3 moved to a position deeper than Phe^{233}, forming a salt bridge with D259 or sometimes with E236. Only for sim-5, did R2 move further, resulting in R2-E236 and R1-E226 salt bridges (Movie 1 of our site).

The translocation of S4 is thought to occur on the order of microseconds (69). To expedite the translocation, we adopted

TABLE 2

Sim. #	Init. Model	Duration (ns)	External field V/nm, direction	Temp.	Vertical movement of C_α (side chain Cz or Nz) of R1, R2, R3, R4, and K5 (in Å)† R1	R2	R3	R4	K5
1	Open	30	0.05, inward	323 K	−1.7 (−0.8)	−0.7 (−0.3)	−0.8 (−2.6)	−0.5 (0.6)	0.0 (−4.9)
2	Open	30	0.05, inward	350 K	−2.5 (−1.9)	−0.9 (−0.8)	−0.7 (−2.2)	−0.8 (0.5)	−0.4 (−4.5)
3	Open	40	0.1, inward	350 K	−4.0 (−2.9)	−4.2 (−7.0)	−6.2 (−9.9)	−5.9 (−9.1)	−5.5 (−12.9)
4	Open	30	0.1, inward	350 K	−3.0 (−1.3)	−4.0 (−4.2)	−6.0 (−9.2)	−5.8 (−9.4)	−5.4 (−11.4)
5	Open	30	0.15, inward	350 K	−4.7 (−6.5)	−7.2 (−14.1)	−8.7 (−17.6)	−7.5 (−14.9)	−5.8 (−12.1)
6	Open	30	0.15, inward	350 K	−5.3 (−5.5)	−4.5 (−4.5)	−5.9 (−7.2)	−6.1 (−10.4)	−5.8 (−10.5)
7	Open	Pore* at 20	0.2, inward	350 K	−11.8 (−15.7)	−14.3 (−21.2)	−14.7 (−24.2)	−10.0 (−17.5)	−4.3 (−11.2)
8	Open	Pore* at 3.3	0.2, inward	350 K			(Not determined)		
9	Resting	30	0.05, outward	350 K	1.7 (1.5)	1.5 (6.4)	0.4 (5.4)	1.2 (3.0)	0.0 (2.3)
10	Resting	20	0.1, outward	350 K	4.7 (3.6)	3.7 (10.5)	1.5 (8.2)	−0.2 (2.4)	−3.2 (−1.4)
11	Resting	Pore* at 23.2	0.2, outward	350 K	6.1 (6.6)	8.0 (14.6)	7.6 (16.2)	5.0 (12.6)	−0.3 (2.4)
12	Resting	Pore* at 4	0.2, outward	350 K			(Not determined)		
13	Resting	10	0.1, inward	350 K	2.8 (3.1)	2.1 (4.6)	0.7 (2.0)	0.7 (3.1)	−2.1 (−3.2)

C_a movement is shown. In the parentheses the movement of Cz, distal carbon atom of side chain is shown. For sim-7 and -11, data just prior to the pore formation are shown.

*Pore means that the membrane broke out and/or a water pore was formed at the indicated time.

†For comparison, vertical movements of Cα-values as reported by Pathak et al. (8) are (in Å): 8.0 for R1, 10.5 for R2, 10.4 for R3, 7.4 for R4, and 1.9 for K5.

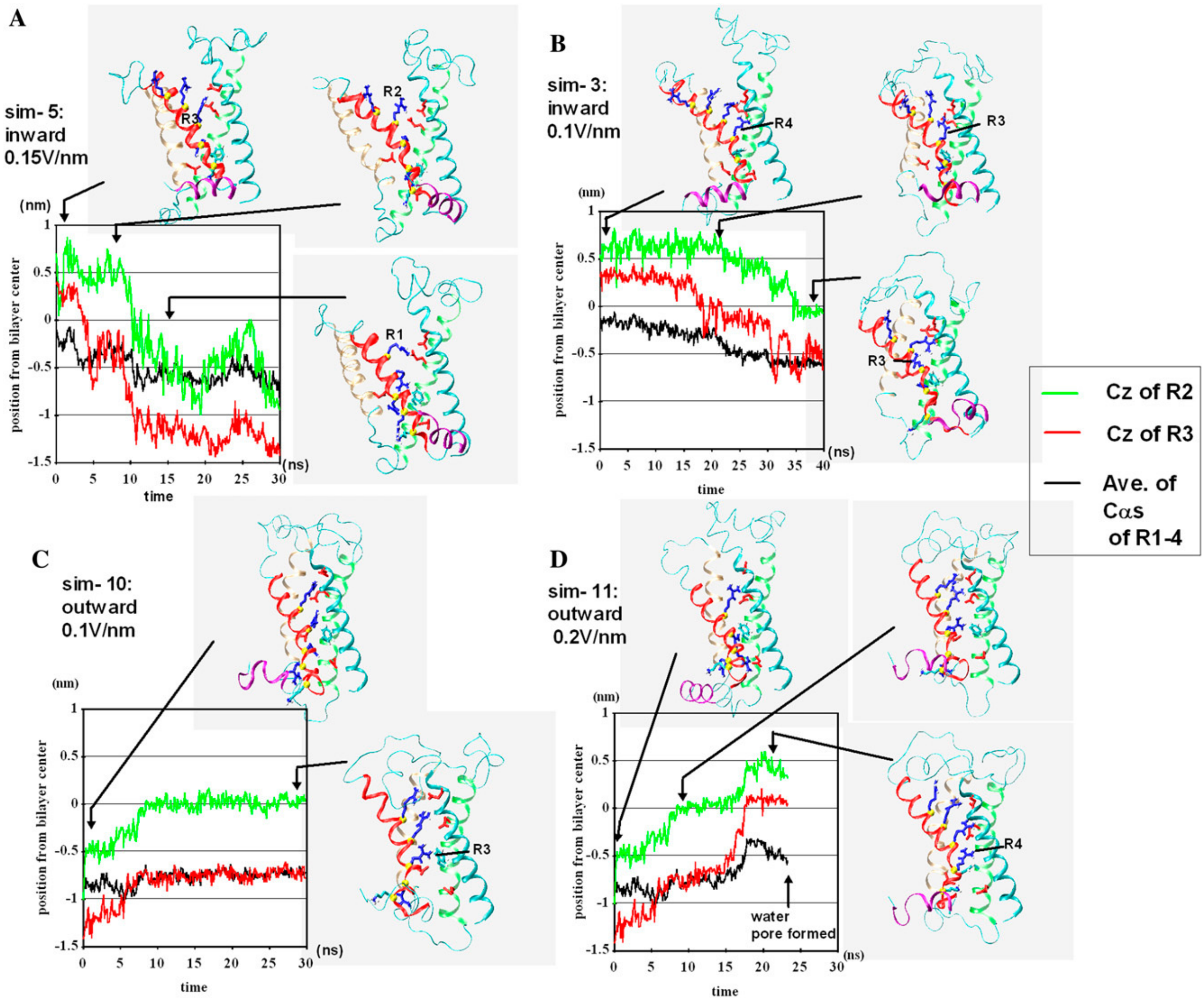

FIGURE 5 Time course of the *z* position for the side chain of R2 and of R3, and the average C_α-value *z* positions of R1–R4. Green and red lines represent the positions of Cz, the carbon atom closest to the charged nitrogen atoms, of R2 and R3, respectively. Black lines show the average C_α-values *z* positions of R1–R4. (*A*) sim-5, (*B*) sim-3, (*C*) sim-10, and (*D*) sim-11.

a high temperature and a strong electric field. In our system, 0.1 V/nm creates the ~800 mV transmembrane potential. Nonetheless, in most of the simulations, the *z* position of S4 as a function of time (Fig. 6) underwent stagnation at intermediate conformations. Inspection of all the simulations showed that both R2-E183/E226 and R3-E183/E226 salt bridges appear to act as barriers slowing down the movement of the S4 helix to a similar degree.

Does our semiclosed structure (sim-5) represent the resting state? In our semiclosed structure, R2 is located fairly inward (Fig. 4 *B*) and is consistent with the recent results of disulfide bonding experiments of the resting state, showing the proximity of R1 and I177 (of S1) as well as I230 (of S2) (21). The Cd^{2+} metal bridge formation study suggested that R1 and I230 approach each other at 6–8 Å in the closed state (21). The C_β-C_β distances in our semiclosed structure are 12.6 Å for R1-I177 and 11.7 Å for R1-I230, respectively. Moreover, in the studies of the ''omega current'' (70), Isacoff and colleagues have shown that E283 in *Shaker* (i.e., E226 in Kv1.2) is positioned near R1 (R362 in *Shaker*, i.e., R294 in Kv1.2) in the closed state. Consistent with this, for our semiclosed structure, the centers of mass of E226 and that of R1 are 5.3 Å apart.

The resting state model (8) places S4 at a very deep position; the C_α of R1 is placed 10.15 Å deeper (inside) than that of E226 of S2, whereas R2 is positioned close to E236 and D259. Compared with their model, our semiclosed structure places the C_α-values of R1–R4 at a relatively high (outside) position, whereas the side chains have moved ahead and are directed inward (Table 2, Fig. 5). However, when we continued the sim-5 to 30 ns, the S4 was still moving inward (Fig. 5 *A*, *black line*). Moreover, in sim-7, a larger S4 translocation was observed than in sim-5, although the membrane broken at 20 ns (Table 2, Fig. 6). Therefore, it seems possible that our semiclosed structure is an interme-

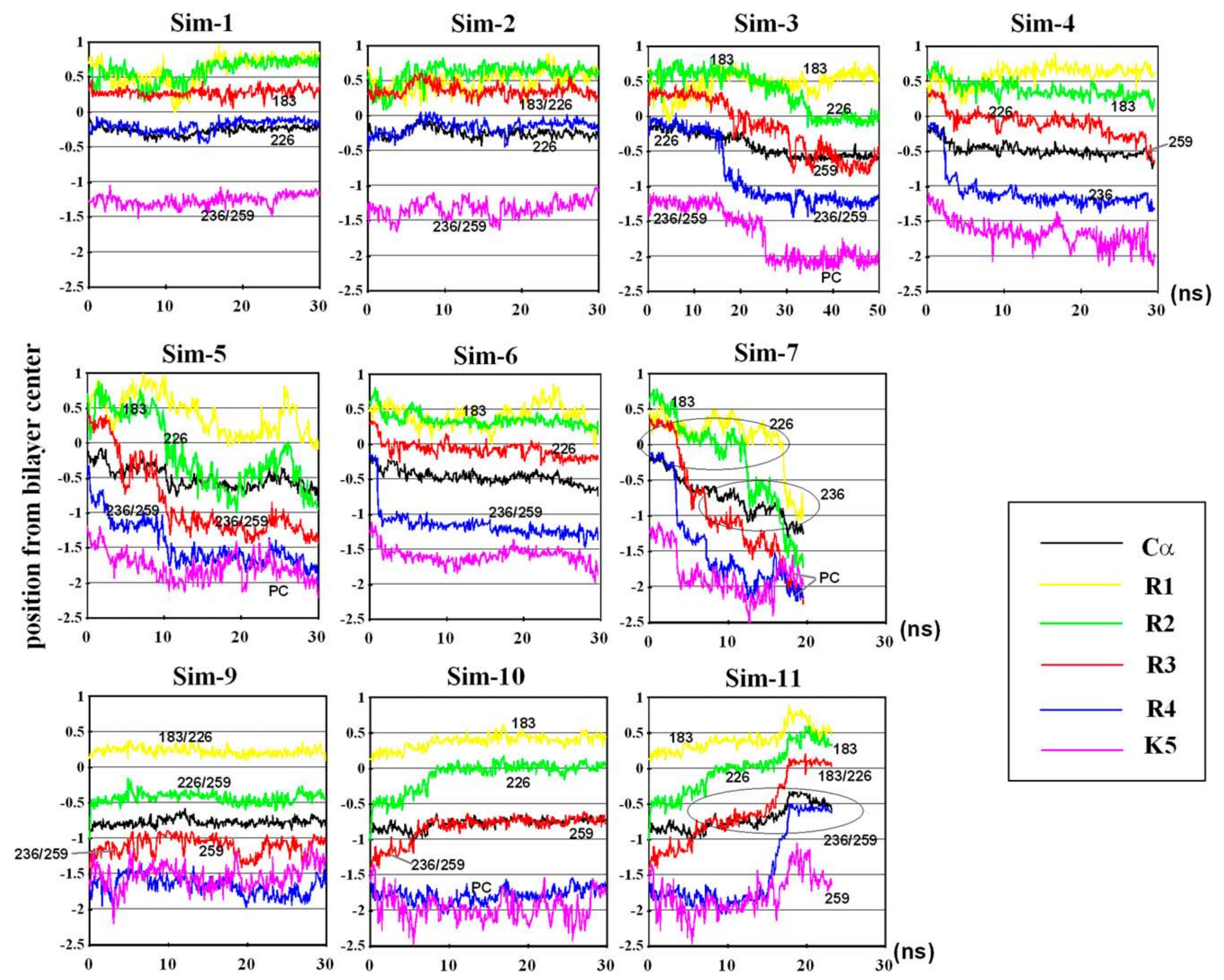

FIGURE 6 Time course of the z position for the side chain of R1–R4 and K5 and the average C_α-value *z* positions of R1–R4. Shown are the results for all the simulations listed in Table 2. Yellow, green, red, and blue lines indicate the *z* positions of the Cz of R1, R2, R3, and R4, respectively, and the magenta line indicates that of the Nz of K5. Black lines show the average of C_α-value *z* positions of R1–R4. The numbers drawn in the graphs show the residues with which R1–R4 and K5 form salt bridges: 183 is E183; 226 is E226; 236 is E236; and 259 is D259. *PC* denotes the DPPC headgroup.

diary structure in which S4 has moved to the midpoint; when simulations on a much longer timescale are performed, further inward S4 movement could be observed. On the other hand, when we performed backward (inward) simulations starting from the resting state model reported in Pathak et al. (8), R1 and R2 exhibited an ~2–3 Å outward translocation, despite the application of an inward electric field (sim-13 of Table 2). This type of simulation could be informative for evaluation of different resting state models. More computational analyses are necessary to understand the resting state structure because subtle conditions of a simulation (such as the use of S5 and S6 helices, lipid types and initial conformations, etc.) influence the results.

S4 movement with outward electric field

We also carried out forward simulations, starting from the closed state model proposed by Pathak et al. (8). In the equilibration run without an electric field, R1 interacted with E226, whereas R2 interacted with both D259 and E236 (Fig. 5, *C* and *D*). In sim-10 (with outward 0.1 V/nm), the outward S4 movement occurred but the magnitude was small (Fig. 5 *C*, Movie 2 of our site, and Fig. 6). At ~5 ns, R2 moved farther upward, and interacted with E226, whereas R1 interacted with E183. At 10 ns, S4 is at an even higher position, with R3 located higher than D259 and E236 and interacting with both of them. R4 and K5 maintained their interaction with the lipid headgroups of the inner membrane leaflet, staying away from the S1 and S2 helices (Movie 2 of our site). Under our conditions, it was rare that R4 (or K5) approached D259 or E236. In sim-11, R4 formed a salt bridge with D259 (Fig. 5 *D* and Movie 3 of our site), although this result should be interpreted carefully because the R4 interaction with D259 occurred immediately before the occurrence of membrane distortion and the pore formation (Movie 3). Overall, these findings again support the view that salt bridges slow down and punctuate the S4 outward translocation, as in the case of the inward translocation.

Environment of the gating charges

The x-ray structure of the Kv1.2 channel shows the R1 and R2 side chains projecting into the hydrophobic lipid acyl chains (5). Simulation studies show that R1 and R2 side chains are hydrated and directed to the external water crevices (8,31,32). Our data support these previous results. The atoms forming hydrogen bonds with R1 and R2 are somewhat similar to R1 in the LFR peptide. In particular, R2 in S1–S4 simulations in the semiclosed state formed hydrogen bonds both with water molecules and OC atoms, as in the case of R1 in LFR, LWR, LLR, and LVR (data not shown). Cumulative radial distribution of molecule types (or groups) as a function of distance from the residue center of each gating-charge-carrying arginine residue also supports this feature (not shown).

We also examined the environment change upon the transition from the open state conformation to the intermediate conformation with the S4 helix displaced 2 Å inward. The results are summarized as follows. For R1, the transition caused the detachment of R1 from the lipid acyl chains, OC and OS atoms. For R2, detachment from the lipid acyl chain, OC and OS, upon transition was more prominent. (However, the prevalence of interactions of R1 and R2 with OC and OS atoms should be carefully interpreted because the particular force field as well as lipid composition chosen in this study may have promoted such interactions.) After the transition, R2 exhibited more involvement of phosphate oxygen atoms in hydrogen-bond formation, similar to LLR and LVR. Because R3 and R4 form hydrogen bonds only with water and/or amino-acid side chains of residues of S1–S3 helices, involvement of OC, OS, and PO_4 were negligible.

Why is R instead of K favored as the gating-charge-carrying residue at the positions R1–R4 of Kv1.2? Although this is difficult at present to answer, two features may be relevant. First, the bidentated (forklike) structure of the guanidinium group of arginine may help make the overall interaction of S4 with S1 and S2 stable. For the intermediate states found, R3 and R4 form 0.78 and 1.46 salt bridges on average with the negatively charged residues, respectively (S4/0.1V/nm of Fig. S2 in Supplementary Material and data not shown). When we replaced R1–R4 with K and performed a similar simulation, fewer salt bridges formed (0.47 for K3 and 0.51 for K4) and the time period without any salt bridge increased (S4K/0.1V/nm in Fig. S2). Because, in general, Rs as opposed to Ks appear to make interactions smooth and constant, it would be interesting to examine whether or not the variance of magnitude of S4 movement among simulation runs is reduced by Rs. Second, we note that Ks introduced in place of R2 and R3 exhibit stronger water-drawing-in effect than Rs. Our inspection and radial distribution function analyses show that K tends to interact strongly with a small number of water molecules forming a cluster in the vicinity of the K residue (~3–4.5 Å from the amino group of the K side chain) (Fig. S3 in Supplementary Material). By contrast, R usually interacts with several water molecules loosely associated with each other and the guanidinium group, forming a loose cluster at a distance of ~4–7 Å from the guanidinium group (Fig. S3). When Ks were introduced as the gating-charge-carrying residue, the density of water at the depth of I230 and F233 was greater than when Rs are used (data not shown). It seems possible that the tight interaction of Ks and water may cause frequent occurrence of proton wire or water channel phenomenon, which would be detrimental to the cellular pH control. We surmise that because of these two features (i.e., the unstable formation of salt bridges and the tight interaction with water), K is not as suitable to the gating-charge carrying as R.

Focused electric field and arginine contribution for gating current

For the *Shaker* and Kv2.1 K^+ channels, channel opening is coupled to displacement of 3 or 4*e* per voltage sensor across the membrane-voltage difference (7,71,72). A number of experimental approaches have suggested the formation of a focused transmembrane electric field (16,19,73–75). This concept is supported by theoretical investigation (31,32). Such a focused electric field should allow a limited translocation of the S4 segment to suffice for voltage-gating. We carried out electrostatic potential calculations for estimating the voltage drop that each R1–R4 and K5 undergo during sim-5. As described in Simulation Details, two conformations were used; in the first simulation S4 was restrained in the open state, in the second S4 was restrained in the semiclosed state (Fig. S4 in Supplementary Material). (The voltage drop for each residue was calculated from each distinct simulation in which the charge of the corresponding residue was turned off.) The results supported the view that the transmembrane electric field is focused at a narrow space near the extracellular side of the membrane. As has been pointed out (31,48), the electric potential was high in the region consisting of lipid headgroup of the outer leaflet of the membrane (Fig. S4). Based on the sim-5 30-ns simulation, the gating charge carried by each charged residue was as follows: R1, 0.01*e*; R2, 0.23*e*; R3, 0.28*e*, R4, 0.57*e*, and K5, 0.34*e*, the sum of which amounts to 1.43*e*. Based on the sim-7 (for the period during which the membrane was intact), R1, 0.40*e*; R2, 0.17*e*; R3, 0.28*e*; R4, 0.42*e*; K5, 0.43*e* and the sum was 1.70*e*. These values are comparable to those reported by Pathak et al. (8): R1, 0.23*e*; R2, 0.61*e*; R3, 0.65*e*; and R4, 0.33*e*, which amount to 1.82*e*. Given that, for R1–R4, our semiclosed model (sim-5) appears to account for ~77% of the C_α movements compared with the models given in Pathak et al. (8) and the side-chain movement is also likely to contribute in our simulation, the sum (1.43*e*) appears reasonable. However, it should also be kept in mind that our use of a very strong electric field may cause a nonphysiological distortion of the electrostatic potential map.

Phe^{233} has been implicated for the hydrophobicity separating the external and internal water vestibule. Inspection of trajectories shows that for the salt-bridge remodeling, for example, from R3-E226 to R3-E236, R3 has to proceed across the Phe^{233}, which is acting as a barrier. Because both arginine and phenylalanine have large side chains, it appears that Phe^{233} has to ''step aside to make a room'' for Rs passing. On the other hand, the presence of D259 facilitates the Rs translocation; from E226, Rs can use D259 as a transit for further movement to E236.

S4 movement supportive of helical screw model

The traditional helical screw or sliding helix models of voltage-gating argued that S4 was moving inside a hydrophilic pore formed mainly by protein residues (11,76). This movement was confirmed by chemical-labeling studies (16,68). It is now established that a narrow waist was protected from the labeling reaction leading to the concept that the gating charges of S4 move through a narrow pathway between the internal and external water vestibules (77). However, analysis of motions of substituted fluorescence probes using several distinct strategies has shown that there is only a small (2–4 Å) outward translocation during gating (14,20). The small translocation led the authors to suggest the transporter model (14). However, more recent disulfide bonding and Cd^{2+} metal bridge experiments (21) led the authors to predict an ~6.5 Å vertical movement of S4 (and ~180° axial rotation).

In our backward simulations, the translocation was ~6.7 Å for sim-5 and ~11 Å for sim-7 (Table 2; note that the membrane broke at 20 ns for sim-7). In terms of S4 axial rotation, sim-5 and sim-7 showed ~90° and ~70° rotation, respectively, whereas sim-11 (forward simulation) exhibited ~80° rotation. However, it is possible that the complete translocation and axial rotation occurs on a much longer timescale, and that we did not cover the full range of motions. More extended simulations may be helpful to examine the range of axial rotation.

Our results show that the direction of the S4 movement is not vertical, but rather tilted. In our simulation, the tilt angle was more flat in the open (activated) state. Therefore, while the luminescence resonance energy transfer data was consistent with the 2 Å vertical displacement of S4 (20), it seems possible that the top of the S4 moves outward upon transition to the open state.

A recent model by Pathak et al. proposed that the S1–S4 domain undergoes an overall counterclockwise rotation when viewed from the extracellular side (8). If this is the case, then we would expect the S4-S5 linker to bend toward S4 itself such that the linker and S3 get closer. In our simulation, such bending was not observed. The S4-S5 linker also rotated, but this appeared to be secondary to the screwlike rotation of S4. However, in our system the S4-S5 linker has a free end, so we cannot address the question how the S4 and S4-S5 linker behave when connected to the pore domain. Future computational studies should include the effect of this S4-S5 linker on the pore domain conformation.

Implications for gating kinetics models

In their early modeling studies of ionic current and channel kinetics, Hodgkin and Huxley (78) represented the kinetics of gating in K channels by the product of independent first-order variables n^4. Here, n represents the fraction of the open gates. In the Hodgkin and Huxley model, four independent and identical K channel subunits were considered to convert individually between a resting state (R) and an activated state (A). In the model, four subunits in the A state make an open channel (O). After the advent of gating-current measurement (79), fluctuation analyses of gating current implied that most of the gating charge for one channel moves in a series of two or three brief steps, suggesting a limited number of voltage-dependent state transitions happen (69,80). This finding and the delay of the S-shape time course of K-channel activation, which was inconsistent with one step-per-subunit models, led Zagotta et al. to introduce a model, namely, the Zagotta-Hoshi-Aldrich model (81). Their work showed that two sequential voltage-dependent conformational changes per subunit can account for many characteristics of steady state and kinetic behavior of Kv channels (71). The Zagotta-Hoshi-Aldrich model was considered with nonindependent transitions between subunits, such as cooperative transitions and concerted conformational changes, and with slow kinetics for the first closing transition (81). In-depth review is beyond the scope of this work, but additional states and explicit concerted transition steps have also been proposed (e.g., (82,83)).

To grasp general trends quickly, we chose 350 K and a strong electric field (0.05–0.2 V/nm), which are obviously not physiological. Even in such harsh conditions, the S4 translocation proceeded in a punctuated manner; S4 was caught in one of the definable conformations and underwent an abrupt change to the next conformation. For both forward and backward simulations, substantial residential time for the conformation including the R3-E183/E226 interaction and that with the R2-E183/E226 interaction was observed. In these harsh conditions they appeared to have a similar degree of stability, although these intermediate conformations may exhibit a difference in stability in physiologically more relevant conditions. It is tempting to envisage that one of the conformations, or both, could be the intermediate conformational state introduced in the Zagotta-Hoshi-Aldrich model. Further computational approaches varying the temperature and voltage could be helpful in characterizing the intermediate states.

CONCLUSION

The N-terminal segment of S4 consists of hydrophobic residues and four arginine residues. Our analyses of interactions between S4 and the DPPC membrane imply that the peptide has energetically compromised characteristics interacting with lipid membrane; arginine favors shallow positioning (and hydration) but hydrophobic residues favor deep positioning (dehydration). It is likely that the hydrophobicity acts to push the arginines deep into the lipid headgroups (i.e., near carbonyl oxygen atoms). The at-every-three-residue rule of arginine places the C_α of R1 and R4 on opposing sides of the helix, which appears to press R1 and R4 into the membrane interior. The deep positioning of R1 is likely to be the prerequisite for the wide-range movement upon voltage change.

In Results and Discussion, we carried out simulations of the S1–S4/DPPC system to examine the effect of an external electric field on the movement of S3 and S4 helices relative to S1 and S2. Although a strong electric field and a high temperature were used, the magnitude of S4 movement was large (with $\sim$6.7 Å vertical translocation). As S4 moves, the gating-charge-carrying arginine residues make serial interaction with negatively charged residues in S1, S2, and S3. The S4 movement occurred in a punctuated manner because the R2-E183/E226 and R3-E183/E236 salt bridges conferred stability to the intermediate conformations. This stability slows down the gating activation dynamics and divides the full voltage-dependent transition into a series of smaller transitions. This is reminiscent of kinetic models such as the Zagotta-Hoshi-Aldrich model, which argue that ''more than one conformational change must occur sequentially per subunit, to open the channel'' (81). Our studies also provide a hypothesis for the basis of a preferred occurrence of R as opposed to K in a voltage sensor. The relatively constant interactions with the negatively charged residues and loose interaction with water molecules may provide arginine suitability for the voltage sensing role. More quantitative analyses, such as free energy profile analysis for S4 movement, are necessary for rigorous assessment of the intermediate conformations. It should also be noted that, for our system, S4 was truncated after the S4-S5 linker and therefore we cannot address the question how S4 movement influences the structure of the pore domain. It also remains to be studied how transitions within one subunit are coupled with the transitions in another subunit. Many more experimental and computational analyses are necessary to address these issues.

SUPPLEMENTARY MATERIAL

To view all of the supplemental files associated with this article, visit www.biophysj.org.

We acknowledge Dr. Yarov-Yarovoy for the coordinates of the Kv1.2 open and resting state models.

REFERENCES

1. Hille, B. 2001. Ion Channels of Excitable Membranes, 3rd Ed. Sinauer, Sunderland, MA.
2. Jan, L. Y., and Y. N. Jan. 1997. Voltage-gated and inwardly rectifying potassium channels. *J. Physiol.* 505:267–282.
3. Li-Smerin, Y., and K. J. Swartz. 1998. Gating modifier toxins reveal a conserved structural motif in voltage-gated Ca^{2+} and K^+ channels. *Proc. Natl. Acad. Sci. USA.* 95:8585–8589.
4. Jiang, Y., A. Lee, J. Chen, V. Ruta, M. Cadene, B. T. Chait, and R. MacKinnon. 2003. X-ray structure of a voltage-dependent K^+ channel. *Nature.* 423:33–41.
5. Long, S. B., E. B. Campbell, and R. Mackinnon. 2005. Crystal structure of a mammalian voltage-dependent *Shaker* family K^+ channel. *Science.* 309:897–903.
6. del Camino, D., and G. Yellen. 2001. Tight steric closure at the intracellular activation gate of a voltage-gated K^+ channel. *Neuron.* 32:649–656.
7. Aggarwal, S. K., and R. MacKinnon. 1996. Contribution of the S4 segment to gating charge in the *Shaker* K^+ channel. *Neuron.* 16:1169–1177.
8. Pathak, M. M., V. Yarov-Yarovoy, G. Agarwal, B. Roux, P. Barth, S. Kohout, F. Tombola, and E. Y. Isacoff. 2007. Closing in on the resting state. *Neuron.* 56:124–140.
9. Jiang, Y., V. Ruta, J. Chen, A. Lee, and R. MacKinnon. 2003. The principle of gating charge movement in a voltage-dependent K^+ channel. *Nature.* 423:42–48.
10. Long, S. B., X. Tao, E. B. Campbell, and R. MacKinnon. 2007. Atomic structure of *s* voltage-dependent K^+ channel in a lipid membrane-like environment. *Nature.* 450:376–382.
11. Catterall, W. A. 1988. Structure and function of voltage-sensitive ion channels. *Science.* 242:50–61.
12. Gandhi, C. S., and E. Y. Isacoff. 2002. Molecular models of voltage sensing. *J. Gen. Physiol.* 120:455–463.
13. Lecar, H., H. P. Larsson, and M. Grabe. 2003. Electrostatic model of S4 motion in voltage-gated ion channels. *Biophys. J.* 85:2854–2864.
14. Chanda, B., O. K. Asamoah, R. Blunck, B. Roux, and F. Bezanilla. 2005. Gating charge displacement in voltage-gated ion channels involves limited transmembrane movement. *Nature.* 436:852–856.
15. Ruta, V., J. Chen, and R. MacKinnon. 2005. Calibrated measurement of gating-charge arginine displacement in the KvAP voltage-dependent K^+ channel. *Cell.* 123:463–475.
16. Yang, N., and R. Horn. 1995. Evidence for voltage-dependent S4 movement in sodium channels. *Neuron.* 15:213–218.
17. Bezanilla, F. 2000. The voltage sensor in voltage-dependent ion channels. *Physiol. Rev.* 80:555–592.
18. Lainé, M., M. C. Lin, J. P. Bannister, W. R. Silverman, A. F. Mock, B. Roux, and D. M. Papazian. 2003. Atomic proximity between S4 segment and pore domain in *Shaker* potassium channels. *Neuron.* 39:467–481.
19. Starace, D. M., and F. Bezanilla. 2004. A proton pore in a potassium channel voltage sensor reveals a focused electric field. *Nature.* 427:548–553.
20. Posson, D. J., P. Ge, C. Miller, F. Bezanilla, and P. R. Selvin. 2005. Small vertical movement of a K^+ channel voltage sensor measured with luminescence energy transfer. *Nature.* 436:848–851.
21. Campos, F. V., B. Chanda, B. Roux, and F. Bezanilla. 2007. Two atomic constraints unambiguously position the S4 segment relative to S1 and S2 segments in the closed state of *Shaker* K channel. *Proc. Natl. Acad. Sci. USA.* 104:7904–7909.
22. Cuello, L. G., D. M. Cortes, and E. Perozo. 2004. Molecular architecture of the KvAP voltage-dependent K^+ channel in a lipid bilayer. *Science.* 306:491–495.
23. Ramu, Y., Y. Xu, and Z. Lu. 2006. Enzymatic activation of voltage-gated potassium channels. *Nature.* 442:696–699.
24. Schmidt, D., Q. X. Jiang, and R. MacKinnon. 2006. Phospholipids and the origin of cationic gating charges in voltage sensors. *Nature.* 444:775–779.

25. Sands, Z. A., and M. S. Sansom. 2007. How does a voltage sensor interact with a lipid bilayer? Simulations of a potassium channel domain. *Structure*. 15:235–244.

26. Ash, W. L., M. R. Zlomislic, E. O. Oloo, and D. P. Tieleman. 2004. Computer simulations of membrane proteins. *Biochim. Biophys. Acta*. 1666:158–189.

27. Gumbart, J. Y., A. Wang, E. Aksimentiev, and K. Schulten. 2005. Molecular dynamics simulations of proteins in lipid bilayers. *Curr. Opin. Struct. Biol.* 15:423–431.

28. Kandt, C., W. L. Ash, and D. P. Tieleman. 2007. Setting up and running molecular dynamics simulations of membrane proteins. *Methods*. 41:475–488.

29. Sotomayor, M., and K. Schulten. 2007. Single-molecule experiments in vitro and in silico. *Science*. 316:1144–1148.

30. Freites, J. A., D. J. Tobias, and S. H. White. 2006. A voltage-sensor water pore. *Biophys. J.* 106:L90–L92.

31. Treptow, W., and M. Tarek. 2006. Environment of the gating charges in the Kv1.2 *Shaker* potassium channel. *Biophys. J.* 90:L64–L66.

32. Jogini, V., and B. Roux. 2007. Dynamics of the Kv1.2 voltage-gated K^+ channel in a membrane environment. *Biophys. J.* 93:3070–3082.

33. Sands, Z., A. Grottesi, and M. S. P. Sansom. 2006. The intrinsic flexibility of the Kv voltage sensor and its implications for channel gating. *Biophys. J.* 90:1598–1606.

34. Järver, P., and Ű. Langel. 2006. Cell-penetrating peptides—a brief introduction. *Biochim. Biophys. Acta*. 1758:260–263.

35. Rothbard, J. B., T. C. Jessop, R. S. Lewis, B. A. Murray, and P. A. Wender. 2004. Role of membrane potential and hydrogen bonding in the mechanism of translocation of guanidinium-rich peptides into cells. *J. Am. Chem. Soc.* 126:9506–9507.

36. Zaro, J. L., and W.-C. Shen. 2003. Quantitative comparison of membrane transduction and endocytosis of oligopeptides. *Biochem. Biophys. Res. Commun.* 307:241–247.

37. Nishizawa, M., and K. Nishizawa. 2007. Molecular dynamics simulations of a stretch-activated channel inhibitor GsMTx4 with lipid membranes: two binding modes and effects of lipid structure. *Biophys. J.* 92:4233–4243.

38. Tieleman, D. P., and H. J. C. Berendsen. 1996. Molecular dynamics simulations of fully hydrated DPPC with different macroscopic boundary conditions and parameters. *J. Chem. Phys.* 105:4871–4880.

39. Berendsen, H. J. C., J. P. M. Postma, W. F. van Gunsteren, and J. Hermans. 1981. Intermolecular Forces, Interaction Models for Water in Relation to Protein Hydration. D. Reidel Publishing, Dordrecht, The Netherlands.

40. Monticelli, L., K. M. Robertson, J. L. MacCallum, and D. P. Tieleman. 2004. Computer simulation of the KvAP voltage-gated potassium channel: steered molecular dynamics of the voltage sensor. *FEBS Lett.* 564:325–332.

41. Freites, J. A., D. J. Tobias, G. von Heijne, and S. H. White. 2005. Interface connections of a transmembrane voltage sensor. *Proc. Natl. Acad. Sci. USA*. 102:15059–15064.

42. Nishizawa, M., and K. Nishizawa. 2006. Interaction between K^+ channel gate modifier hanatoxin and lipid bilayer membranes analyzed by molecular dynamics simulation. *Eur. Biophys. J.* 35:373–381.

43. Bemporad, D., Z. A. Sands, C. L. Wee, A. Grottesi, and M. S. Sansom. 2006. Vstx1, a modifier of Kv channel gating, localizes to the interfacial region of lipid bilayers. *Biochemistry*. 45:11844–11855.

44. Yarov-Yarovoy, V., D. Baker, and W. A. Catterall. 2006. Voltage sensor conformations in the open and closed states in ROSETTA structural models of K^+ channels. *Proc. Natl. Acad. Sci. USA*. 103: 7292–7297.

45. Hess, B., H. Bekker, H. J. C. Berendsen, and J. G. E. M. Fraaije. 1997. LINCS: a linear constraint solver for molecular simulations. *J. Comput. Chem.* 18:1463–1472.

46. Darden, T., D. York, and L. Pedersen. 1993. Particle mesh Ewald: an $N\log(N)$ method for Ewald sums in large systems. *J. Chem. Phys.* 98:10089–10092.

47. Berendsen, H. J. C., J. P. M. Postma, W. F. van Gunsteren, A. DiNola, and J. R. Haak. 1984. Molecular dynamics with coupling to an external bath. *J. Chem. Phys.* 81:3684–3690.

48. Tieleman, D. P. 2004. The molecular basis of electroporation. *BMC Biochem.* 5:10.

49. Sotomayor, M., V. Vásquez, E. Perozo, and K. Schulten. 2007. Ion conduction through MscS as determined by electrophysiology and simulation. *Biophys. J.* 92:886–902.

50. Humphery, W., A. Dalke, and K. Schulten. 1996. VMD—visual molecular dynamics. *J. Mol. Graph.* 14:33–38.

51. Aksimentiev, A., and K. Schulten. 2005. Imaging α-hemolysin with molecular dynamics: ionic conductance, osmotic permeability, and the electrostatic potential map. *Biophys. J.* 88:3745–3761.

52. Sachs, J. N., P. S. Crozier, and T. B. Woolf. 2004. Atomistic simulations of biologically realistic transmembrane potential gradients. *J. Chem. Phys.* 121:10847–10851.

53. Hessa, T., H. Kim, K. Bihlmaier, C. Lundin, J. Boekel, H. Andersson, I. Nisson, S. H. White, and G. von Heijne. 2005. Recognition of transmembrane helices by the endoplasmic reticulum translocon. *Nature*. 433:377–381.

54. Hessa, T., S. H. White, and G. von Heijne. 2005. Membrane insertion of a potassium-channel voltage sensor. *Science*. 307:1427.

55. Dorairaj, S., and T. W. Allen. 2007. On the thermodynamic stability of a charged arginine side chain in a transmembrane helix. *Proc. Natl. Acad. Sci. USA*. 104:4943–4948.

56. Peled-Zehavi, H., I. T. Arkin, D. M. Engelman, and Y. Shai. 1996. Coassembly of synthetic segments of *Shaker* K^+ channel within phospholipid membranes. *Biochemistry*. 35:6828–6838.

57. Mattila, K., R. Kinder, and B. Bechinger. 1999. The alignment of a voltage-sensing peptide in dodecylphosphocholine micelles and in oriented lipid bilayers by nuclear magnetic resonance and molecular modeling. *Biophys. J.* 77:2102–2113.

58. MacCallum, J. L., W. F. D. Bennet, and D. P. Tieleman. 2007. Partitioning of amino acid side chains into lipid bilayers: results from computer simulations and comparison to experiment. *J. Gen. Physiol.* 129:371–377.

59. Allen, T. W. 2007. Modeling charged protein side chains in lipid membranes. *J. Gen. Physiol.* 130:237–240.

60. Roux, B. 2007. Lonely arginine seeks friendly environment. *J. Gen. Physiol.* 130:233–236.

61. Chavan, M., A. Yan, and W. J. Lennarz. 2005. Subunits of the translocon interact with components of the oligosaccharyl transferase complex. *J. Biol. Chem.* 280:22917–22924.

62. Chavan, M., Z. Chen, G. Li, H. Schindelin, W. J. Lennarz, and H. Li. 2006. Dimeric organization of the yeast oligosaccharyl transferase complex. *Proc. Natl. Acad. Sci. USA*. 103:8947–8952.

63. Nilsson, I. M., and G. von Heijne. 1993. Determination of the distance between the oligosaccharyltransferase active site and the endoplasmic reticulum membrane. *J. Biol. Chem.* 268:5798–5801.

64. Murata, Y., H. Iwasaki, M. Sasaki, K. Inaba, and Y. Okamura. 2005. Phosphoinositide phosphatase activity coupled to an intrinsic voltage sensor. *Nature*. 435:1239–1243.

65. Sasaki, M., M. Takagi, and Y. Okamura. 2006. A voltage sensor-domain protein is a voltage-gated proton channel. *Science*. 312:589–592.

66. Ramsey, I. S., M. M. Moran, J. A. Chong, and D. E. Clapham. 2006. A voltage-gated proton-selective channel lacking the pore domain. *Nature*. 440:1213–1216.

67. Tiwari-Woodruff, S. K., C. T. Schulteis, A. F. Mock, and D. M. Papazian. 1997. Electrostatic interactions between transmembrane segments mediate folding of *Shaker* K^+ channel subunits. *Biophys. J.* 72:1489–1500.

68. Larsson, H. P., O. S. Baker, D. S. Dhillon, and E. Y. Isacoff. 1996. Transmembrane movement of the *Shaker* K^+ channel S4. *Neuron*. 16:387–397.

69. Conti, F., and W. Stühmer. 1989. Quantal charge redistributions accompanying the structural transitions of sodium channels. *Eur. Biophys. J.* 17:53–59.

70. Tombola, F., M. M. Pathak, and E. Y. Isacoff. 2005. Voltage-sensing arginines in a potassium channel permeate and occlude cation-selective pores. *Neuron.* 45:379–388.

71. Zagotta, W. N., T. Hoshi, and R. W. Aldrich. 1994. *Shaker* potassium channel gating. III: Evaluation of kinetics models for activation. *J. Gen. Physiol.* 103:321–362.

72. Seoh, S. A., D. Sigg, D. M. Papazian, and F. Bezanilla. 1996. Voltage-sensing residues in the S2 and S4 segments of the *Shaker* K^+ channel. *Neuron.* 16:1159–1167.

73. Baker, O. S., H. P. Larsson, L. M. Mannuzzu, and E. Y. Isacoff. 1998. Three transmembrane conformations and sequence-dependent displacement of the S4 domain in *Shaker* K^+ channel gating. *Neuron.* 20:1283–1294.

74. Asamoah, O. K., J. P. Wuskell, L. M. Loew, and F. A. Bezanilla. 2003. Fluorometric approach to local electric field measurements in a voltage-gated ion channel. *Neuron.* 37:85–97.

75. Ahern, C. A., and R. Horn. 2005. Focused electric field across the voltage sensor of potassium channels. *Neuron.* 48:25–29.

76. Guy, H. R., and P. Seetharamulu. 1986. Molecular model of the action potential sodium channel. *Proc. Natl. Acad. Sci. USA.* 83:508–512.

77. Nguyen, T. P., and R. Horn. 2002. Movement and crevices around a sodium channel S3 segment. *J. Gen. Physiol.* 117:436–469.

78. Hodgikin, A. L., and A. F. Huxley. 1952. A quantitative description of membrane current and its application to conduction and excitation in nerve. *J. Physiol.* 117:500–544.

79. Armstrong, C. M., and F. Bezanilla. 1973. Currents related to movement of the gating particles of the sodium channels. *Nature.* 242:459–461.

80. Sigg, D., E. Stefani, and F. Bezanilla. 1994. Gating current noise produced by elementary transitions in *Shaker* potassium channels. *Science.* 264:578–582.

81. Zagotta, W. N., T. Hoshi, J. Dittman, and R. W. Aldrich. 1994. *Shaker* potassium channel gating. II: transitions in the activation pathway. *J. Gen. Physiol.* 103:279–319.

82. Schoppa, N. E., and F. J. Sigworth. 1998. Activation of *Shaker* potassium channels. III. An activation gating model for wild-type and V2 mutant channels. *J. Gen. Physiol.* 111:313–342.

83. Kanevsky, M., and R. W. Aldrich. 1999. Determinants of voltage-dependent gating and open-state stability in the S5 segment of *Shaker* potassium channels. *J. Gen. Physiol.* 114:215–242.